ECS Transactions, 58 (2) 173-181 (2013)
10.1149/05802.0173ecst ©The Electrochemical Society

Increasing Conductivity in Proton Conductors $BaCeO_{3-\delta}$ doped with Pr

J. F. Basbus[a], A. Caneiro[b], and L. V. Mogni.[b]

[a] Departamento Caracterizacion de Materiales, Centro Atomico Bariloche, AGNPCyT, CNEA, Bariloche, Rio Negro, 8400, Argentina
[b] Departamento Caracterizacion de Materiales, Centro Atomico Bariloche, CNEA, CONICET, Bariloche, Rio Negro, 8400, Argentina

In this work we explore the effect of partial substitution of Ce for Pr ions in $BaCe_{1-x}Pr_xO_{3-\delta}$ ($0 \leq x \leq 0.8$) perovskites with the aim of increasing the oxygen vacancies concentration and H^+ charge carriers. The oxides were obtained by Pechini combustion method and sintered at 1350°C. The Pr incorporation improves the capability of to obtain dense samples at this temperature. Crystal structure were studied by X-ray diffraction, while morphology by SEM. The conductivity was studied by Electrical Impedance Spectroscopy (EIS) under 20 % O_2/Ar and 10 % H_2/Ar, both with 2% humidity. We found that the Pr content diminished the lattice parameters, increase the sintering capacity and the conductivity under wet oxidant atmosphere, but it decreases the stability under reducing atmosphere.

Introduction

Oxygen vacancies in $BaCeO_{3-\delta}$ perovskite could be hydrated according to the following reaction:

$$V_O^{\bullet\bullet} + H_2O + O_O^x \rightarrow 2OH^{\bullet} \quad (1)$$

In this compound, the proton conductivity is due to the hopping of H^+ ions through O sublattice. This mechanism of ionic conductivity is characterized by their low activation energy (1) and the proton solubility which increases as T decreases (2). These features would allow observing ionic conductivity at temperatures below 400 °C. Therefore, these kinds of oxides are suitable for application such as sensors, H-permeable membranes and electrolytes for Protonic Conductors Solid Oxide Fuel Cell (PC-SOFC) (2-3). These applications are interesting because they improve the energy conversion efficiency and allow the production of high purity H_2. However, the effort of materials science is focused to develop new oxides with better properties, improving the ionic conductivity, the long term stabilities, and decreasing the cost of processing materials.

Reaction (1) depends on vapor pressure (pH_2O) and oxygen vacancies concentration ($V_O^{\bullet\bullet}$) in the solid. Then, replacing Ce^{+4} for lanthanides Ln^{+3} ions should be the way to increase the oxygen vacancies concentration in $BaCeO_{3-\delta}$:

$$2Ce_{Ce}^x + O_O^x + Ln_2O_3 \rightarrow 2Ln_{Ce}^{'} + V_O^{\bullet\bullet} + 2CeO_2 \quad (2)$$

The effect of different substitution in these compounds has been widely studied. It was found that the highest conductivities are achieved for Gd-doped compound (4). This highest ionic conductivity has been attributed to the fact that the Gd-doped composition presents the largest cell volume (5). Therefore, some strategies involving multiple doping will be explored in order to improve the electrolytes performances and extend the stability under CO_2 containing atmospheres. However, while in some cases the lanthanides co-dopant enhances the conductivity (6), in other cases, the doping hampers the proton conductivity. This is because proton conductivity is prevented when unit cell volume decreases (7) or when local symmetry around doped sites increases (8).

Hence, in this work we explore the effect of partial substitution of Ce for Pr ions in $BaCe_{1-x}Pr_xO_{3-\delta}$ ($0 \leq x \leq 0.8$) with the aim of increasing the oxygen vacancies concentration and H^+ charge carriers.

Experimental

The dense electrolytes were obtained through Pechini modified method. The starting materials, $Ba(NO_3)_2$, Pr_6O_{11}, and $Ce(NO_3)_3.6H_2O$, were dissolved using EDTA and citric acid as quelating agents in a molar relation metal:EDTA:Citric acid of 1:1:1.5. Finally the pH was adjusted to 10 using ammonium hydroxide. The polymerization was induced by heating. The obtained polymers were heated until to produce self-combustion. The fine powders were calcined and thermally treated at 900 ºC for 12 h. Resulting powders were uniaxially pressed at 50 kg/cm^2 and sintered at 1350 ºC for 12 hs.

Crystal structure of powders and phase purity were studied by X Ray Diffraction (XRD) using a PANalytical Empyrean diffractometer. The crystalline structures were refined fitting the structural parameters of BaCeO3 (9) by Rietveld method applied to XRD data through Fullprof software (10).

Microstructures of dense samples were studied by Scanning Electronic Microscopy (SEM) with a Philips 515 microscope. The elemental analysis was performed by energy dispersive spectroscopy (EDS).

The thermodynamic stability of compounds was studied by Thermogravimetry (TG) using a Cahn 1000 electrobalance (11) and analyzing the percentage of mass variation as a function of temperature between 100 and 800 ºC in 20 % O_2/Ar and 5 % H_2/Ar atmospheres. During TG measurements, the equilibrium between sample and atmosphere was achieved.

Electrical resistances of dense sample were determined by Electrochemical Impedance Spectroscopy (EIS). Dense disc of samples were painted on both sides with Pt ink. The EIS spectra were collected between 100 and 600 °C under wet (2% H_2O) synthetic air (20 % O_2/Ar) and 10 % H_2/Ar flow, using an Autolab PGSTAT30 potentiostat between 1 MHz and 0.1 Hz, with 50 mV of amplitude. The EIS spectra were fitted using electrical equivalent circuit and the Zview software (12).

Results and Discussion

Samples Characterization

Figure 1 shows, as an example, the XRD pattern of the $BaCe_{0.8}Pr_{0.2}O_{3-\delta}$ perovskite. All samples present a single phase, corresponding to the orthorhombic space group *Pmcn*, Nº 62 (9,13). Table 1 summarizes the cell parameters. As could be observed *a*, *b* and *c* orthorhombic lattice parameters decrease as the Pr content increases. The starting material, Pr_6O_{11} presents two Pr^{+4} for each Pr^{+3}. Therefore, it could be expected that, while Pr^{+4} ions substitute Ce^{+4} in B sites (r_{Ce+4}^{VI}= 0.87 Å), the Pr^{+3} could partially replace both, Ba^{+2} in A site (r_{Ba+2}^{XII}= 1.61 Å) and Ce^{+4} in B site. We expect that the replacement of Ce^{4+} by Pr^{3+} predominates over that of Ba^{2+} by Pr^{3+} due to the stoichiometry of the compound. In that case, the change of lattice parameter with Pr would indicate that two effects compress the structure [13]: The reduction of the mean ionic radii in B site because Pr^{+4} (r_{Pr+4}^{VI}= 0.85 Å) has a slightly smaller ionic radii than the Ce^{+4}, and the creation of oxygen vacancies induced by the charge compensation of Pr^{+3} (r_{Pr+3}^{VI} = 0.99 Å) ions which could distort the lattice, but without causing a change of symmetry. In order to prove these assumptions a detailed crystallographic study confirming the substitution of Ba^{+2} by Pr substitution would be necessary.

Figure 2 shows SEM images of dense electrolytes sintered at 1350°C. BaCeO3-δ composition presents sintered grain with high pores. As Pr content increases, the high pores disappear and the density of the electrolytes improves.

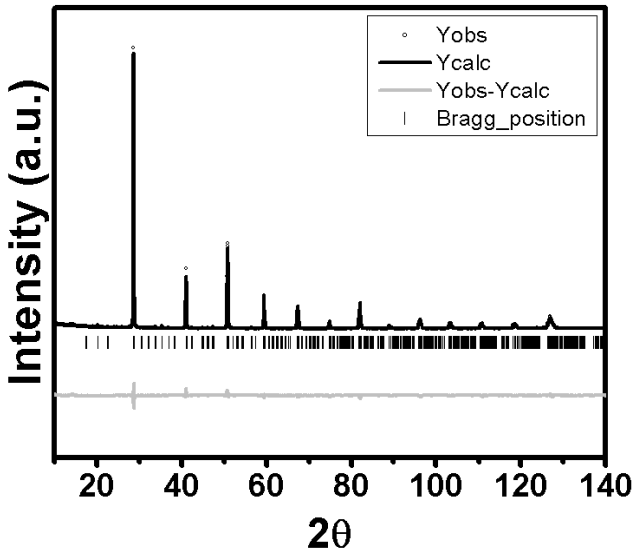

Figure 1. XRD profiles measured (Yobs), calculated (Ycalc) and difference (Yobs-Ycalc) for $BaCe_{0.8}Pr_{0.2}O_{3-\delta}$ perovskite.

TABLE I. Cells parameters of orthorhombic *Pmcn* perovskites.

$BaCe_{1-x}Pr_xO_{3-\delta}$ x	a (Å)	b (Å)	c (Å)
0	8.7727	6.2337	6.2128
0.2	8.7649	6.2281	6.2082
0.4	8.7508	6.2200	6.1975
0.6	8.7499	6.2209	6.1965
0.8	8.7408	6.2152	6.1903

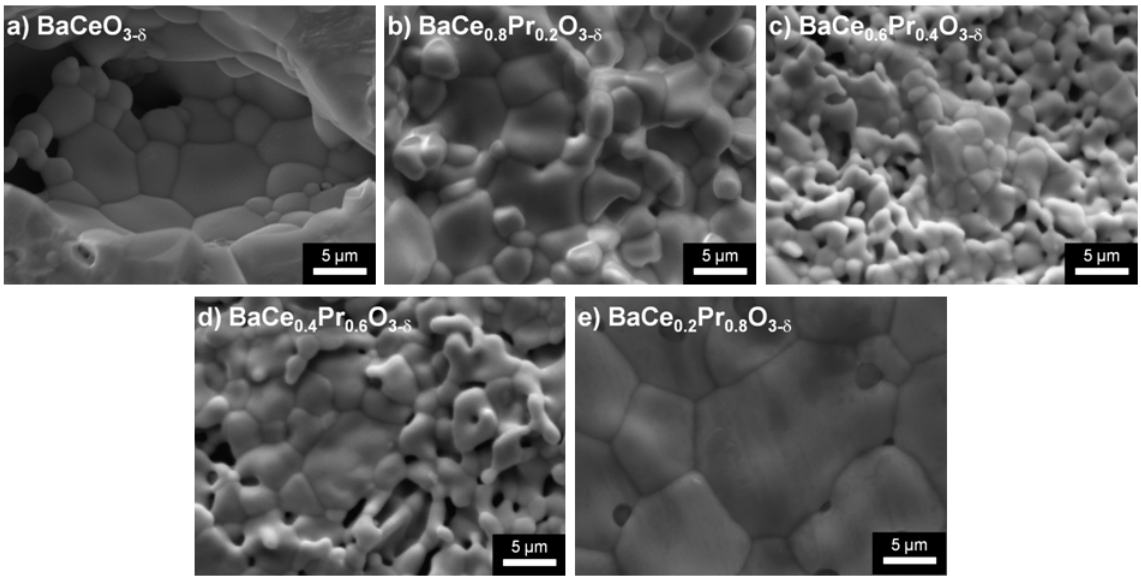

Figure 2. SEM images of dense $BaCe_{1-x}Pr_xO_{3-\delta}$ pellets sintered at 1350°C.

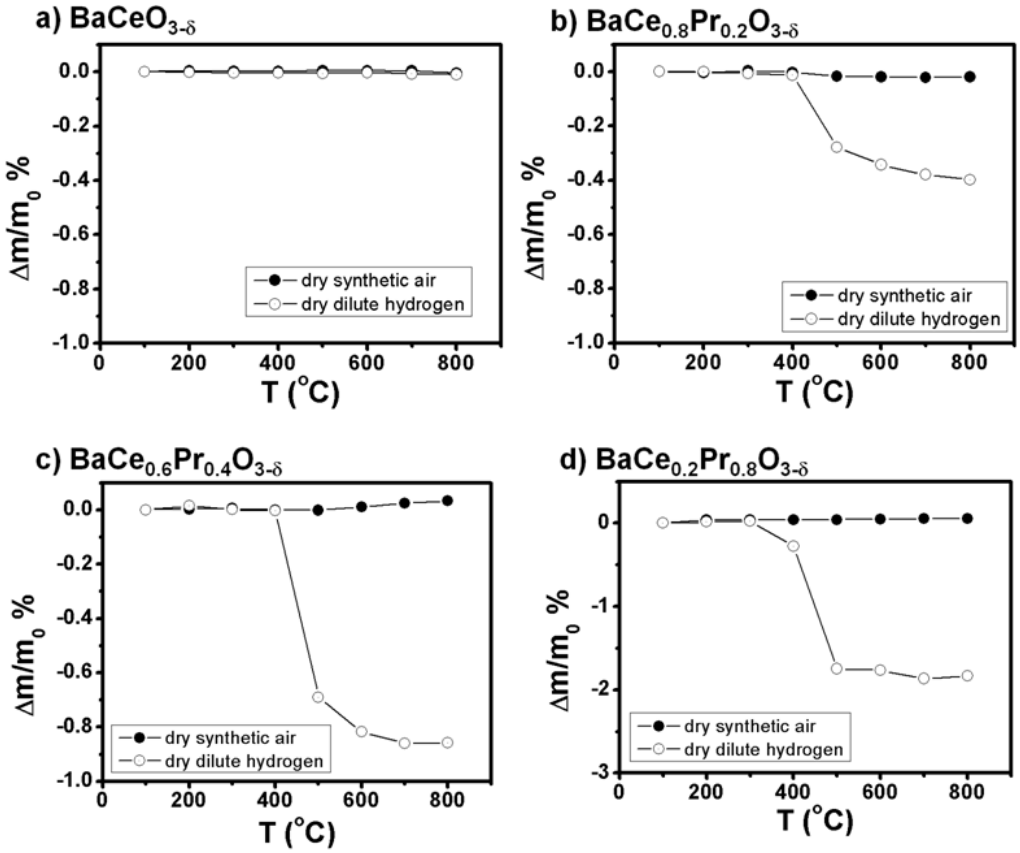

Figure 3. Percent mass variation ($\Delta m/m_0$ %) as a function of temperature in dry synthetic air and dry diluted hydrogen (5%H2/Ar) of a) $BaCeO_{3-\delta}$, b) $BaCe_{0.8}Pr_{0.2}O_{3-\delta}$ c) $BaCe_{0.6}Pr_{0.4}O_{3-\delta}$ and d) $BaCe_{0.2}Pr_{0.8}O_{3-\delta}$ powders.

Thermodynamic Stability

Figure 3 shows the mass variation in percent as a function of T for $BaCe_{1-x}Pr_xO_{3-\delta}$ ($0< x < 0.8$) compounds in air and 10% H_2/Ar. No change of mass was detected in dry synthetic air for all compositions. However, under diluted hydrogen, a progressive decrease of mass can be observed above 400 °C as Pr content increases. This progressive mass change is due to partial reduction of Pr^{+4} into Pr^{+3} .

In order to evaluate if Pr^{+4} reduction affects the crystal structure of $BaCe_{1-x}Pr_xO_{3-\delta,}$ we studied the powders by XRD before and after heat treated at 800 °C during 24 h in 10 % H_2/Ar. Figure 4 shows how the reducing treatment affects the diffration peaks in the high angle region ($2\theta \sim 120\text{-}135^{o}$). From the whole diffraction patterns we could conclude that $BaCeO_{3-\delta}$ and $BaCe_{0.8}Pr_{0.2}O_{3-\delta}$ preserve the orthorhombic structure; $BaCe_{0.6}Pr_{0.4}O_{3-\delta}$ and $BaCe_{0.4}Pr_{0.6}O_{3-\delta}$ change the crystal symmetry and $BaCe_{0.2}Pr_{0.8}O_{3-\delta}$ broad its peaks due to the sample amorphization. Therefore, we could conclude that the Pr content decrease the stability of $BaCe_{01-x}Pr_xO_{3-\delta}$ compounds under reducing atmosphere above 400 °C. This result is similar to those reported by Magrasó et al (15). The change of mass and crystal structure also affects the mechanical integrity of dense pellets due to density variation which induce cracks.

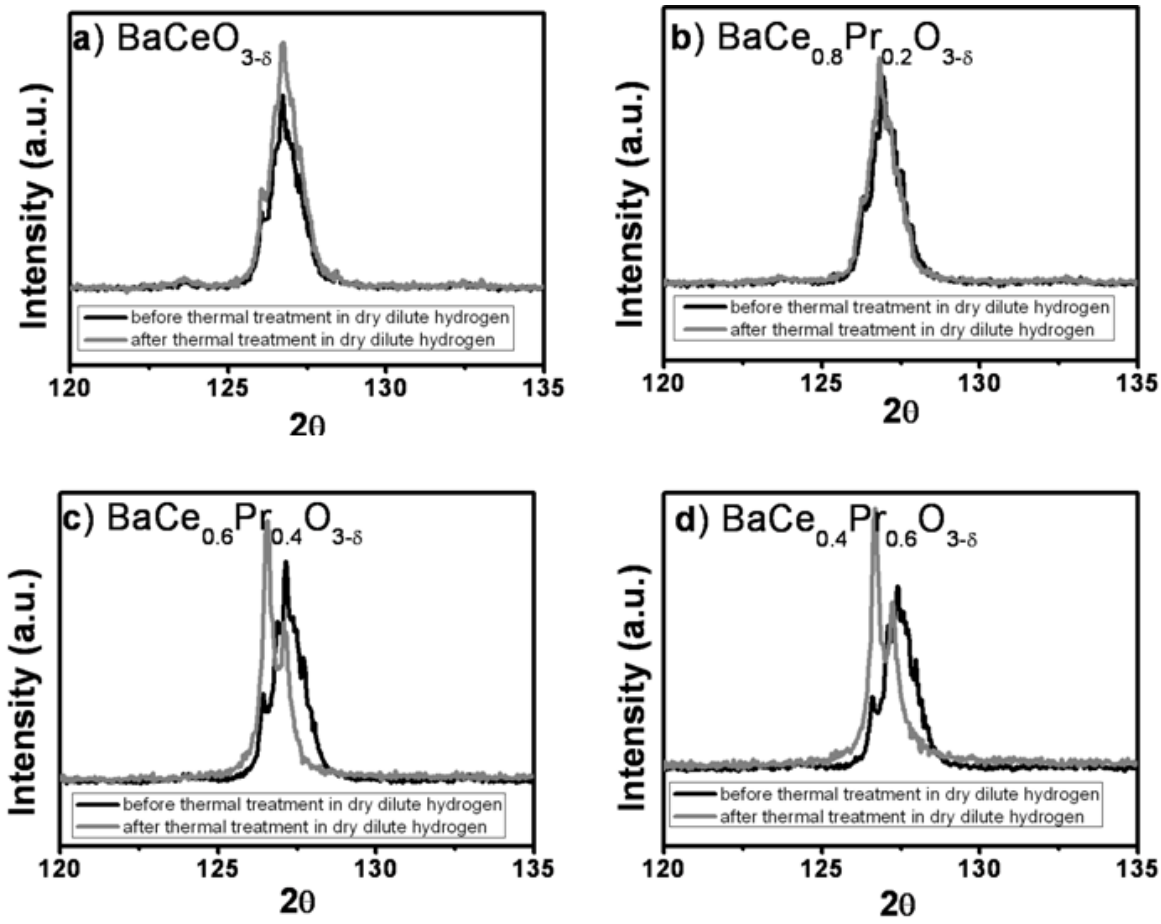

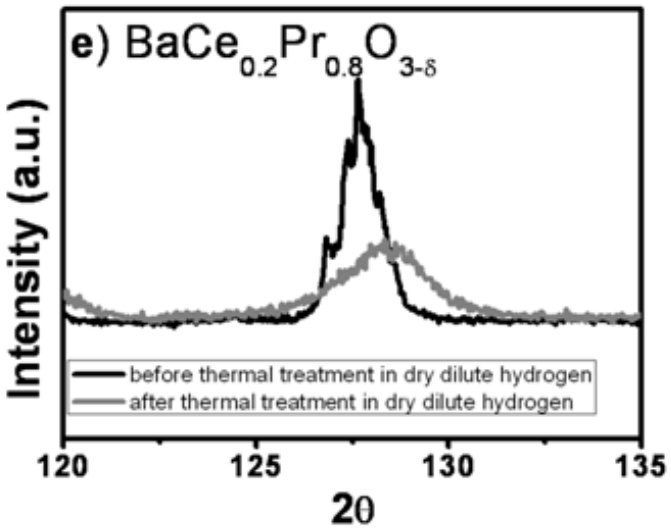

Figure 4. XRD pattern between 120 and 135 º of samples before and after of be heated at 800 ºC in dry 10%H2/Ar for 24 h. a) $BaCeO_{3-\delta}$, b) $BaCe_{0.8}Pr_{0.2}O_{3-\delta}$ c) $BaCe_{0.6}Pr_{0.4}O_{3-\delta}$ and d) $BaCe_{0.2}Pr_{0.8}O_{3-\delta}$.

Characterization of Electrical Conductivity in Wet Air

Figure 5 shows the Nyquist plots of the electrolytes in wet synthetic air at 200 ºC. At low temperatures, we could distinguish two high frequency arcs. These arcs were fitted using an electrical equivalent circuit considering two series circuits, each of them with a resistance in parallel with a phase constant element (Rcpe). These elements were associated with the ionic conductivity through bulk and grain boundary electrolyte contributions. The Pt-electrode response was discarded because it appears at lowest frequency. The electrolyte contributions move thought highest frequencies and the resistances decrease as the temperature increases. Therefore, the overal electrolyte resistance is obtained from the interception of the impedance spectra with the real axis at high frequencies.

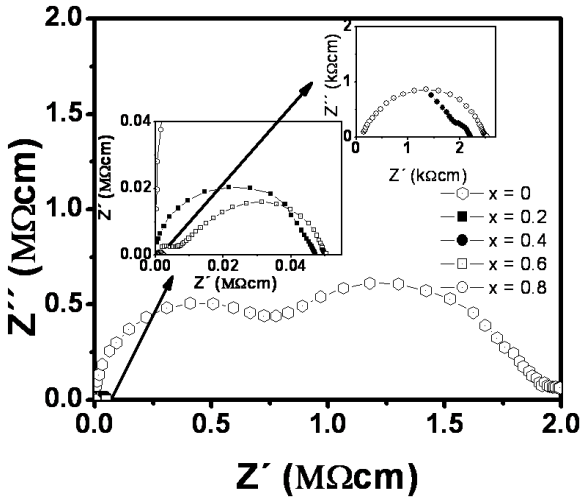

Figure 5. Nyquist plots of EIS spectra for $BaCe_{1-x}Pr_xO_{3-\delta}$ electrolytes obtained at 200 ºC in wet synthetic air.

Figure 6a shows the Arrhenius plot of total electrolyte conductivity: $\sigma = \sigma_b + \sigma_{gb}$, where σ_b is bulk conductivity and σ_{gb} the grain boundary contribution. Pr doping improves the total conductivity decreasing the electrolyte resistance between one and two orders of magnitude and shifting the maximum frequencies of relaxation to higher values. However, the increment of total conductivity is no linear with Pr content (See Figure 6b). The conductivity takes similar values for Pr-rich $BaCe_{1-x}Pr_xO_{3-\delta}$ compositions. One possible explication to this behavior, is that at high Pr content, the Pr^{+3} could partially fill the Ba^{+2} A-site. In this case, the charge compensation of Pr^{+3} demands to fill the oxygen vacancies, lowering the conductivity since the proton incorporation would decrease.

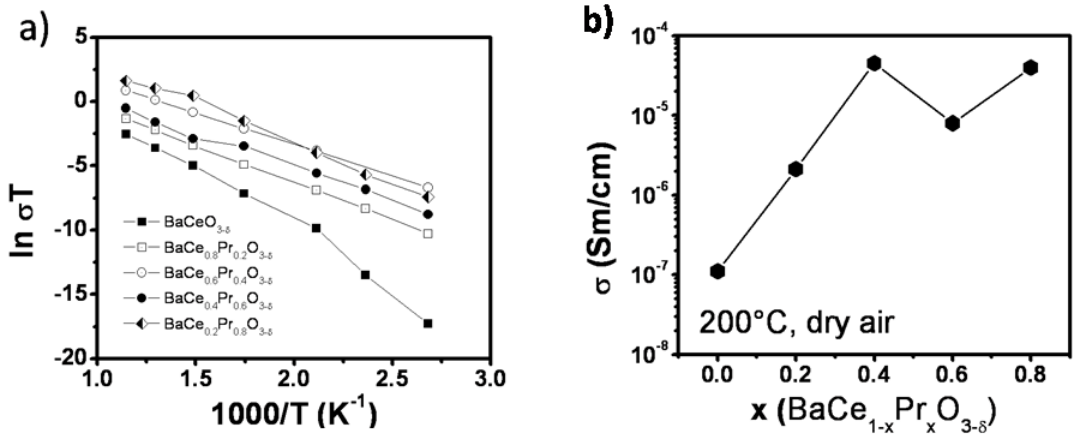

Figure 6. a) Total electrolyte conductivity ($\sigma = \sigma_b + \sigma_{gb}$) Arrhenius plot for each composition. b) Total electrolyte conductivity σ obtained in wet synthetic air as a function of Pr content at 200ºC.

Characterization of Electrical Conductivity in Wet 10% H_2

Considering the thermodynamic stability results discussed above, we studied the electrolyte resistance in wet diluted H_2, only for $BaCeO_{3-\delta}$ and $BaCe_{0.8}Pr_{0.2}O_{3-\delta}$ compositions. Figure 7 shows the Arrhenius plot of total electrolyte conductivity obtained in wet synthetic air and wet 10%H_2/Ar for $BaCeO_{3-\delta}$ (a) and $BaCe_{0.8}Pr_{0.2}O_{3-\delta}$ (b).

$BaCeO_{3-\delta}$ presents the same electrolyte response in both atmospheres, while $BaCe_{0.8}Pr_{0.2}O_{3-\delta}$ increases the electrolyte conductivity under reducing atmosphere. The different behavior would arise from the fact that, while the oxygen non stoichiometry of $BaCeO_{3-\delta}$ remains practically constant with T regardless the atmosphere (see Figure 3a), the $BaCe_{0.8}Pr_{0.2}O_{3-\delta}$ is partially reduced generating both oxygen vacancies and electronic charge carriers. Similar results were obtained for high Pr-doping $BaCe_{0.8-x}Pr_xGd_{0.2}O_{2.9}$, which was proposed as cathode materials due to their mixed H-ionic and electronic conductivities [16]. However, with this information it is difficult to assign the increment of conductivity to H-ionic conductivity, O-ionic conductivity or electronic conductivity. Further studies on blocking electrodes will be necessary to understand the cause of this improvement.

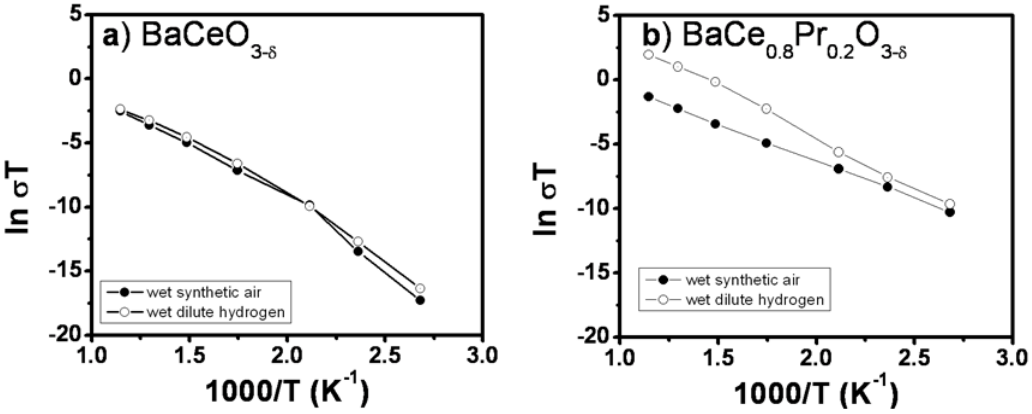

Figure 7 Comparison of Arrhenius plot of total electrolyte conductivity as a function of T obtained in wet synthetic air and wet 10%H_2/Ar for a) $BaCeO_{3-\delta}$ and b) $BaCe_{0.8}Pr_{0.2}O_{3-\delta}$.

Conclusion

Studying the effect of $BaCeO_{3-\delta}$ partial substitution with Pr, we could observe that the main effect on crystal structure was the decreasing of lattice parameter for orthorhombic ***Pmcn*** phase. The Pr incorporation also improve the sintering capability of this electrolytes. From point of view of thermodynamic stability, we could detect that all composition were stables under oxidizing atmosphere, but the instability in reducing atmosphere increases as the Pr content increases.

Besides, we found that the electrolyte resistances increase with Pr doping in both, oxidizing and reducing atmosphere. However, remains unclear if the reason of this behavior is the increasing on protonic, oxygen vacancies or electronic charge carriers.

Acknowledgments

This work was supported by CNEA (Argentine Atomic Energy Commission), CONICET (Argentine Research Council), National University of Cuyo and ANPCyT. The authors thank to the integrants of Division Caracterizacion de Materiales (Centro Atomico Bariloche) for their support and helpful discussion.

References

1. A. Sammells, R. Cook, J. White, J. Osborne and R. MacDuff, *Solid State Ionics* **52,** 111 (1992).
2. K.D. Keuer, *Annu. Rev. Mater. Res.* 33 (2003), p. 333
3. Iwahara, H.; Uchida, H.; Ono, K.; Ogaki, K. *J. Electrochem. Soc.* **135**(2), (1988), p. 529.

4. M. Amsif, D. Marrero-López, J.C. Ruiz-Morales, S.N. Savvin, P. Núñez. *J. Power Sources* **196,** 9154 (2011).
5. J. Kikuchi, S. Koga, K. Kishi, M. Saito, J. Kuwano, *Solid State Ionics* **179,** 1413 (2008).
6. X.T. Su, Q-Z Yan, X-H Ma, W-F Zhang, C-C Ge *Solid State Ionics* **177,** 1041 (2006).
7. C. Zhang, H. Zhao, *Solid State Ionics* **206,** 17 (2012).
8. F. Giannici, A. Longo, K-D Kreuer, A. Balerna, A. Martorana, *Solid State Ionics* **181,** 122 (2010).
9. K. Knight, *Solid State Ionics*, **145,** 275 (2001).
10. http://www.ill.eu/sites/fullprof/
11. A. Caneiro, P. Bavdaz, J. Fouletier, J.P. Abriata, *Rev. Sci. Instrum.*, **53,** 1072 (1982)
12. Zview versión 2.9b. Copyright 1990-2005, Scribner Associates, Inc. D. Johnson
13. K. Knight, *Mater. Res. Bull.*, **30**, 347 (1995)
14. http://abulafia.mt.ic.ac.uk/shannon/ptable.php
15. A. Magrasó, C. Frontera, A. Gunnaes, A. Tarancon, D. Marrero-Lopez, T. Norby, R. Haugsrud; *J. Power Sources*, **196,** 9141 (2011).
16. R. Mukundan, P. K. Davies, and W. L. Worrell, *J. Electrochem. Soc.*, **148**(1) A82 (2001).